



1 **Modeling study of impacts on surface ozone of regional transport and**  
2 **emission reductions over North China Plain in summer 2015**

3 Xiao Han<sup>1,2</sup>, Lingyun Zhu<sup>3</sup>, Shulan Wang<sup>4</sup>, Xiaoyan Meng<sup>5</sup>, Meigen Zhang<sup>1,2</sup>, Jun Hu<sup>4</sup>

4 <sup>1</sup> *State Key Laboratory of Atmospheric Boundary Layer Physics and Atmospheric Chemistry, Institute of*  
5 *Atmospheric Physics, Chinese Academy of Sciences, Beijing 100029, China.*

6 <sup>2</sup> *College of Earth Science, University of Chinese Academy of Sciences, Beijing 100049, China*

7 <sup>3</sup> *Shanxi Province Institute of Meteorological Sciences, Taiyuan 030002, China*

8 <sup>4</sup> *Chinese Research Academy of Environmental Sciences, Beijing, 100012, China*

9 <sup>5</sup> *China National Environmental Monitoring Centre, Beijing, 100012, China*

10

11 Corresponding author:

12 Meigen Zhang

13 LAPC, Institute of Atmospheric Physics, Chinese Academy of Sciences

14 HuaYanBeiLi 40#, Chaoyang District

15 Beijing, China

16 Post code: 100029

17 Tel: 86-010-62379620

18 Fax: 86-010-62041393

19 E-mail: [mgzhang@mail.iap.ac.cn](mailto:mgzhang@mail.iap.ac.cn)

20 Lingyun Zhu

21 E-mail: [mgzhang@mail.iap.ac.cn](mailto:mgzhang@mail.iap.ac.cn)

22

23 Other authors:

24 Xiao Han, E-mail: [hanxiao@mail.iap.ac.cn](mailto:hanxiao@mail.iap.ac.cn)

25 Shulan Wang, E-mail: [shulanwang@foxmail.com](mailto:shulanwang@foxmail.com)

26 Xiaoyan Meng, E-mail: [mengxy@cnemc.cn](mailto:mengxy@cnemc.cn)

27 Jun Hu, E-mail: [hujun@craes.org.cn](mailto:hujun@craes.org.cn)

28

29

30

31

32        **Abstract**

33        Tropospheric ozone ( $O_3$ ) has replaced  $PM_{2.5}$  or  $PM_{10}$  as the premier pollution in the North China Plain  
34 (NCP) during summer in recent years. A comprehensive understanding of the  $O_3$  production in responding  
35 to the reduction of precursor emission over NCP is demanded urgently for the effective control policy  
36 design. In this study, the air quality modeling system RAMS-CMAQ (regional atmospheric modeling  
37 system-community multiscale air quality), coupled with the ISAM (integrated source apportionment  
38 method) module is applied to investigate the  $O_3$  regional transport and source contribution features during  
39 a heavy  $O_3$  pollution episode in June 2015 over NCP. The results show that the emission sources in  
40 Shandong and Hebei were the major contributors to  $O_3$  production in the NCP. Not only more than 50%  $O_3$   
41 mass burden in local regions, but also about 20-30% and 25-40%  $O_3$  mass burdens in Beijing and Tianjin  
42 were contributed by the emission sources in these two provinces, respectively. On the other hand, the urban  
43 areas and most  $O_3$  pollution regions of NCP were mainly dominated by the VOC-sensitive conditions, while  
44 "both control" and  $NO_x$ -sensitive conditions dominated the suburban and remote areas, respectively. Then,  
45 based on the sensitivity tests, the effects of several hypothetical scenarios of emission control on reducing  
46 the  $O_3$  pollution were compared and discussed. The results indicated that the emission control of industry  
47 and residential sectors was the most efficient way if the emission reduction percentage was higher than  
48 40%. However, when the emission reduction percentage dropped below 30%, the power plant sector could  
49 make significant contributions to the decrease in  $O_3$ . The control strategies should be promptly adjusted  
50 based on the emission reduction, and the modeling system can provide valuable information for precisely  
51 choosing the emission sector combination to achieve better efficiency.

52

53

54

55

56

57

58

59

60

61



62

63 **1. Introduction**

64 In addition to the downward injection of stratospheric ozone ( $O_3$ ), tropospheric  $O_3$  is formed via a  
65 suite of photochemical reactions involving nitrogen oxides ( $NO_x$ ), volatile organic compounds (VOCs),  
66 and sunlight.  $O_3$  plays a role in controlling the chemical composition and climate of the troposphere and  
67 harms vegetation and human health, especially in industrialized regions (Kleinman et al., 2002). In recent  
68 years, the emission of  $O_3$  precursors,  $NO_x$  and VOCs, have increased substantially due to the economic  
69 growth, rapid population expansion, and urbanization in the North China Plain (NCP). During the summer,  
70  $PM_{2.5}$  or  $PM_{10}$  are replaced by  $O_3$  as the premier pollution type in major urban areas (China Environmental  
71 Status Bulletin 2015).

72 Numerous studies have investigated the spatial and temporal distribution characteristics of  $O_3$  in the  
73 NCP. Lin et al. (2008) analyzed the three-year observation data of the  $O_3$  mixing ratio at a remote Global  
74 Atmosphere Watch site near Beijing and showed the seasonal variation features of the  $O_3$  background value  
75 for the NCP. Tang et al. (2012) gathered two-year observation data of the  $O_3$  mixing ratio for 22 sites  
76 (located in urban, rural, and coastal areas) during a field campaign in the NCP and coupled the data with  
77 the meteorological parameters from the WRF. The spatial and temporal variations of  $O_3$  were deeply  
78 analyzed, and the  $O_3$ – $NO_x$ –VOCs sensitivity was initially investigated in this study. Ran et al. (2012) and  
79 Dufour et al. (2010) compared the  $O_3$  seasonal variation features in megacities between the NCP and  
80 southern China. On the other hand, several studies have applied the chemistry transport model system to  
81 reproduce the three-dimensional  $O_3$  continuous distribution characteristic and discussed the sensitivity of  
82  $O_3$  to precursor emissions (Wang et al., 2012; Nie et al., 2014).

83 Because of the strong emission of air pollutants, widespread haze clouds caused by serious air  
84 pollution have occurred frequently over the NCP (Tao et al., 2012; Wang et al., 2013; Li et al., 2016; Zhou  
85 et al., 2017). Aiming to solve this problem, the government has executed severe emission control strategies  
86 in recent years (Gao et al., 2016), which have yielded an initial effect. As reported by the China  
87 Environmental Status Bulletin, the mass loadings of sulfur dioxide ( $SO_2$ ),  $NO_2$ ,  $PM_{2.5}$ , and  $PM_{10}$  steadily  
88 fell from 2013 to 2015. However,  $O_3$  has become the only pollutant whose mass burden has continued to  
89 increase in the 74 experimental cities of China. The amount of surface  $O_3$  is expected to continue increasing  
90 as the particulate mass loading decreases due to the emission control strategies employed in the NCP (Deng  
91 et al., 2011). Therefore, there is an urgent need to prevent environmental and health hazards in the NCP



92 resulting from the surface O<sub>3</sub>.

93 As a secondary pollutant, although the basic features of surface O<sub>3</sub> in the NCP are well known from  
94 measurement or modeling studies, understanding the chemical links between O<sub>3</sub> and its two main precursors,  
95 NO<sub>x</sub> and VOC, is important for designing effective pollution reduction strategies (Castell et al., 2009). The  
96 chemical transport model is an indispensable method for resolving the above issue, as it can quantify the  
97 main physical and chemical mechanisms of pollutant formation and transport. Liu et al. (2010) used two  
98 process analysis modules (integrated process rates and integrated reaction rates) embedded in CMAQ to  
99 capture the dynamical and photochemical processes of O<sub>3</sub> formation in 2008 over China. As a result, the  
100 influence and contribution of each important process can be distinguished and quantified. Tang et al. (2017)  
101 also used the integrated process rates module for measurement data from a set of observation stations to  
102 evaluate the sensitivity of O<sub>3</sub> production in June 2008 over the NCP. Xing et al. (2010) developed a  
103 statistical response surface method and coupled it with CMAQ to analyze O<sub>3</sub> sensitivities to NO<sub>x</sub> and VOCs  
104 emission changes in 2005 over eastern China. The overall impacts from individual sources, including  
105 regional NO<sub>x</sub> and VOCs emission sources, have been evaluated using this modeling system. Li et al. (2008)  
106 applied a tagged tracer method to the framework of NAQPMS to identify the transport contributions from  
107 various O<sub>3</sub> production regions to total O<sub>3</sub> levels in 2008 over central eastern China. This method can be  
108 used to eliminate the errors caused by nonlinearities in the transport and fast photochemistry of O<sub>3</sub> and its  
109 precursors.

110 In general, the substantial features of O<sub>3</sub> formation sensitivity and the contributions of regional-scale  
111 transport have been discussed in these studies. However, more work needs to be done to achieve a  
112 comprehensive understanding of O<sub>3</sub> behavior over the NCP, especially the source contribution approaches  
113 of recent years. In this study, an air quality modeling system called RAMS-CMAQ (regional atmospheric  
114 modeling system–community multiscale air quality) that is coupled with the ISAM (integrated source  
115 apportionment method) module is applied to estimate the regional contributions of O<sub>3</sub> among major regions  
116 of the NCP and to quantify the relative amount of O<sub>3</sub> originating from specific VOCs and NO<sub>x</sub> emissions  
117 sources. A unique method that can distinguish the O<sub>3</sub>–NO<sub>x</sub>–VOC sensitivity features is also used to identify  
118 the precursor sensitivity regions and verify the results of the ISAM. In addition, the brute-force method is  
119 applied to investigate the effect of reducing anthropogenic emissions on the O<sub>3</sub> mass burden. Therefore, the  
120 precursor control type and contribution from specific geographic areas and emission sectors can be obtained,  
121 and some valuable information can be provided for control strategies in the NCP.



122

123 **2. Methodology**

124 CMAQ (version 5.0.2), released in April 2014 by the US EPA  
125 ([https://www.airqualitymodeling.org/index.php?title=CMAQ\\_version\\_5.0.2\\_\(April\\_2014\\_release\)\\_Techn](https://www.airqualitymodeling.org/index.php?title=CMAQ_version_5.0.2_(April_2014_release)_Technical_Documentation&oldid=587)  
126 [ical\\_Documentation&oldid=587](https://www.airqualitymodeling.org/index.php?title=CMAQ_version_5.0.2_(April_2014_release)_Technical_Documentation&oldid=587)), was applied over the NCP for 2-month simulations in January and June  
127 2015. Several updates and revisions, such as the chemical process corresponding to NH<sub>3</sub> and SO<sub>2</sub> and the  
128 secondary aerosol formation of SOA (secondary organic aerosol) and nitrate, have been added in this  
129 version. The updated and expanded version of the carbon bond mechanism (CB05) (Sarwar et al., 2008)  
130 and the sixth-generation modal CMAQ aerosol model (AERO6) were applied to simulate the gas-phase  
131 chemistry mechanisms and formation and the dynamic processes of aerosols, respectively. The  
132 ISORROPIA model (version 1.7) was used to describe the thermodynamic equilibrium of gas-particle  
133 transformation (Nenes et al., 1999). The highly versatile RAMS numerical code (Cotton et al., 2003), which  
134 can well simulate the boundary layer and the underlying surface, is utilized to provide the meteorological  
135 fields for CMAQ. The anthropogenic emissions of major pollution species (NO<sub>x</sub>, SO<sub>2</sub>, VOCs, BC, OC,  
136 primary PM<sub>2.5</sub>, and PM<sub>10</sub>) were obtained from the monthly-based emission inventory, with 0.25°×0.25°  
137 horizontal resolution and four categories (industry, power, transport, and residential), which were developed  
138 to support the Model Intercomparison Study Asia (Li et al., 2015). The original version of this emission  
139 inventory was developed for Asia as a contribution to the TRACE-P (Transport and Chemical Evolution  
140 over the Pacific) Mission and ACE-Asia (Asian Pacific Regional Aerosol Characterization Experiment)  
141 (Streets et al., 2003). Additionally, the NO<sub>x</sub> and NH<sub>3</sub> emissions from the soil and natural hydrocarbon  
142 emissions were obtained from the Global Emissions Inventory Activity 1°×1° global monthly inventory  
143 (Benkovitz et al., 1996). The Global Fire Emissions Database, Version 3 (FGEDv3.0; van der Werf et al.,  
144 2010), was applied to provide the biomass burning emissions from wildfires, savanna burning, and slash-  
145 and-burn agriculture. The VOCs and nitrogen oxides from flight exhaust, lighting, paint, fossil fuel, and  
146 other sectors were obtained from the regional emission inventory in Asia (REAS, Version 2,  
147 <http://www.jamstec.go.jp/frsgc/research/d4/emission.htm>) and the emission database for global  
148 atmospheric research (Olivier et al., 1994), respectively.

149 The ISAM module was used to track O<sub>3</sub> from different geographic regions and source types. This  
150 source apportionment tool was developed from the TSSA (Wang et al., 2009) in an early version of the  
151 CMAQ model. Compared with the previous version, the ISAM improved the approach for the advection of



152 tagged tracers and the tracking of precursor reactions and increased the flexibility of the application by  
153 minimizing the amount of data preparation (Kwok et al., 2013). An updated piecewise parabolic algorithm  
154 was applied to reasonably estimate the major dynamics processes, including advection transport, vertical  
155 diffusion, and dry deposition. For the nonlinear gas-phase chemical interactions, which are important for  
156 O<sub>3</sub> formation, a hybrid approach that employs the direct sensitivity methods as linear equations using lower  
157 and upper triangular matrices, which is known as LU decomposition (Yang et al., 1997), was applied for  
158 description. In addition, the ISAM uses two tracers for individual nitrogen and VOC species to represent  
159 the O<sub>3</sub> chemical formation regime attributed to either NO<sub>x</sub> or VOC emission sources. As described by Kwok  
160 et al. (2014), the total concentration of O<sub>3</sub> in each model grid cell is equal to the sum of O<sub>3</sub> tracers that were  
161 produced in either VOC- or NO<sub>x</sub>-sensitive conditions:

$$162 \quad O_{3 \text{ bulk}} = \sum_{\text{tag}} O_3 V_{\text{tag}} + \sum_{\text{tag}} O_3 N_{\text{tag}} \quad (1)$$

163 where O<sub>3</sub>V<sub>tag</sub> and O<sub>3</sub>N<sub>tag</sub> are the VOC-sensitive and NO<sub>x</sub>-sensitive O<sub>3</sub> attributed to each tag source,  
164 respectively. Therefore, the contribution from VOCs or NO<sub>x</sub> can be tracked individually, and the precursor  
165 control types in each grid can be deduced. Detailed information regarding the ISAM can be found in Kwok  
166 et al. (2013).

167 The simulation has two layer grids. The coarse domain covers East Asia (Figure 1, D1), with a  
168 horizontal grid distance of 64 km and a total area of 6654 km×5440 km, and an inner domain (Figure 1,  
169 D2) with a 16 km×16 km resolution is two-way nested with the outer one. The inner domain covers the  
170 major regions of the NCP, including the megacity of Beijing, Tianjin, the capital city of the Shijiazhuang  
171 province, Jinan, the industrial town of Tangshan, and the Hebei, Shandong, and Shanxi provinces. The  
172 simulation used 15 vertical levels, of which nearly half were concentrated in the lowest 2 km, to improve  
173 the simulation of the atmospheric boundary layer. Numerous previous studies have demonstrated that this  
174 modeling system performs well in simulating the pollutant mass concentrations (Zhang et al., 2006; Han et  
175 al., 2014; Han et al., 2016)

176

### 177 3. Model evaluation

178 The meteorological parameters, such as the temperature and wind field, are important impact factors  
179 of ozone formation and transport. Therefore, the daily average temperature, relative humidity, wind speed,  
180 and maximum wind direction in January and June 2015 were compared with the surface observation data  
181 (released by the Chinese National Meteorological Center: <http://data.cma.cn/>) for Beijing, Tianjin,



182 Shijiazhuang, and Jinan. The comparison results are shown in Figure 2. The modeled temperature and  
183 relative humidity are shown to generally coincide with the observations at all four of these stations, except  
184 that some of the extreme high or low values appeared abruptly. The modeled wind speed, which could  
185 reproduce the higher value in Tianjin and Jinan and lower value in Beijing and Shijiazhuang, also followed  
186 the magnitude of observations well. However, a direct comparison between observed and modeled data is  
187 difficult, especially for the wind vector, which can be easily influenced by the surrounding surface features.  
188 The modeled and observed wind directions were not in good agreement with each other. Nevertheless, the  
189 north wind in winter and south wind in summer were generally captured by the simulation results for all  
190 stations.

191 The modeled mass concentrations of  $O_3$  and one of its precursors ( $NO_2$ ) were compared with the hourly  
192 observation data from the Ministry of Environmental Protection of China; the results are shown in Figures  
193 3 and 4. The statistical parameters – the means, standard deviation, and correlation coefficients between the  
194 observations and simulations – are listed in Tables 1 and 2. The nitrogen oxide and tropospheric ozone were  
195 two kinds of typical trace gases with high chemical activity and relatively short lifetimes. The diurnal  
196 change in Figures 3 and 4 is obvious, and the distinctive values of the mass concentrations between different  
197 seasons can also be found. The simulation results also reproduced these important features, especially the  
198 evident diurnal variation of  $O_3$  at these four stations. The mass concentration of  $O_3$  in summer was generally  
199 higher than that in winter because of the strong photochemistry during the daytime in summer. On the other  
200 hand, the simulation results were able to capture most of the pollution episodes during these two months,  
201 but the model still struggled to reflect some of the extreme high mass burden of the observations, such as  
202 the high value points that appeared on June 22 and 25 in Beijing and on January 20 in Shijiazhuang. The  
203 metrics listed in Tables 1 and 2 were used to evaluate the model performance, following the study of Yu et  
204 al. (2006). Most of the correlation coefficients were higher than 0.5 for  $NO_2$  and 0.6 for  $O_3$ , which indicates  
205 that the model performed well in reproducing the observation trend. In addition, the standard deviations  
206 between the observation and simulation of  $NO_2$  and  $O_3$  were also similar in most cases, except for  $NO_2$  in  
207 January. Figure 3 shows that the model missed many of the high values of observation that appeared during  
208 the first half of January. In addition to the possible deficiency of the emission inventory, the model may not  
209 adequately simulate the chemistry mechanism of nitrogen transformation during winter over the NCP.  
210 However, this underestimation of  $NO_2$  did not influence the performance of the  $O_3$  simulation, as the mean  
211 and standard deviation between the observation and simulation results were relatively close. The largest



212 deviation of the modeled O<sub>3</sub> mean, which was higher than that of the observation, appeared at Tianjin in  
213 June, with the overestimation that occurred during June 16-18, as shown in Figure 3. Yu et al. (2010)  
214 reported similar results and noted that the model might not well resolve the titration by NO in an urban area  
215 under a low O<sub>3</sub> mass burden background by applying both the CB05 and SAPRC-99 mechanisms. ~~The~~  
216 ~~slight overestimation could also be found at other stations.~~ Nevertheless, the comparison generally showed  
217 that the model could basically reproduce the meteorological field and mass concentration and trends of O<sub>3</sub>  
218 and its precursor NO<sub>2</sub> during different seasons over the NCP.

219

#### 220 4. Results and discussion

221 The surface spatial distributions of the monthly average values of the modeled NO<sub>x</sub>, VOCs, and  
222 maximum daily 8-hour average O<sub>3</sub> mass concentration (8H-O<sub>3</sub>) for January and June 2015 are shown in  
223 Figure 5. The monthly average wind field is also shown. The diffusion condition is shown to have been  
224 weak due to the obviously smaller wind speed over Beijing, Tianjin, Hebei, Shandong, and northern Henan  
225 in both January and June. In addition to the strong emission, this observation should be the main reason for  
226 the high mass burden of NO<sub>x</sub> and VOCs in these regions. In addition, the maximum values were mainly  
227 concentrated in the urban areas of the NCP during these two months, including the following five major  
228 pollution cities: Beijing, Tianjin, Shijiazhuang, Jinan, and Tangshan. However, the distribution patterns  
229 between O<sub>3</sub> and the precursors were significantly different, which indicates that the formation and transport  
230 processes of O<sub>3</sub> should be complex in the NCP. Unlike the seasonal variation of NO<sub>x</sub> and VOCs, the mass  
231 burden of O<sub>3</sub> in summer was obviously higher than that in winter because of the stronger photochemical  
232 activity. The 8H-O<sub>3</sub> mass concentration, which exceeded the Grade II standard (160 μg m<sup>-3</sup>), was  
233 widespread throughout southern Beijing, Hebei and almost the entire areas of Tianjin and Shandong, with  
234 values reaching 180-200 μg m<sup>-3</sup> in the tri-province area of Hebei, Shandong, and Henan in June. The serious  
235 O<sub>3</sub> pollution was mainly concentrated in the northwest part of the Shandong province.

236 The contribution of O<sub>3</sub> from the major NCP regions, including Beijing, Hebei, Shandong, Tianjin, and  
237 Shanxi, was calculated using ISAM-CMAQ-RAMS; the results are shown in Figure 6 (NS: NO<sub>x</sub>-sensitive  
238 O<sub>3</sub>) and Figure 7 (VS: VOC-sensitive O<sub>3</sub>). The total percentage can be obtained by summing the  
239 contributors of NS and VS. The distribution patterns of NS and VS contributions were generally similar to  
240 each other. The mass contribution of O<sub>3</sub> in Shandong, Hebei, and Shanxi was mainly contributed by local  
241 sources, and the total percentage generally exceeded 50%. However, the local sources did not provide the





242 primary contributions in Beijing and Tianjin, and the regional contributions from Hebei and Shandong  
243 could exceed 30% in these two cities, respectively. This feature clearly indicates that the regional transport  
244 of precursors should be an important factor of O<sub>3</sub> pollution in Beijing and Tianjin. The contribution from  
245 Shanxi to other regions was very small due to the hindrance to pollutant transport provided by the Taihang  
246 Mountains, which are located to the east of the Shanxi province. In addition, the contribution from  
247 Shandong provided at least more than 65% to the mass burden of O<sub>3</sub> in the Bohai Sea. This feature explains  
248 the source of the large value that appears over this area in Figure 4. On the other hand, the contribution of  
249 VS was obviously higher than that of NS in Beijing, Tianjin, Hebei, and Shandong. Compared with the NS,  
250 the percentage of VS was generally double in Beijing and Tianjin and more than 10% higher in all of  
251 Shandong and the southern part of Hebei. In contrast, the contribution of NS was clearly higher than that  
252 of VS in Shanxi, which means that the major role of the O<sub>3</sub> formation in Shanxi should be different from  
253 that in other regions.

254 To distinguish the O<sub>3</sub>–NO<sub>x</sub>–VOC sensitivity features, a method that is suitable for the results of three-  
255 dimensional chemistry/transport models was applied to identify the precursor sensitivity regions in the NCP.  
256 In addition to the base case, two sensitivity tests, which can reduce 30% of the VOC emissions or 30% of  
257 the NO<sub>x</sub> emissions within the entire model domain, were conducted. Then, the deviation of the maximum  
258 daily 8H-O<sub>3</sub> between the base case and these two sensitivity tests could be utilized to determine the  
259 precursor control types in each grid. Here, we used  $\Delta O_{3V}$  and  $\Delta O_{3N}$  to represent the variation of the mass  
260 concentration of O<sub>3</sub> due to the reduction in VOC or NO<sub>x</sub> emission, respectively (Sillman and West, 2009):  
261 (1) if the changes in  $\Delta O_{3V}$  and  $\Delta O_{3N}$  were both less than 4  $\mu\text{g m}^{-3}$ , this grid was likely controlled by neither  
262 NO<sub>x</sub> nor VOCs; (2) if  $\Delta O_{3N}$  increased to a value greater than 4  $\mu\text{g m}^{-3}$  and  $\Delta O_{3V}$  decreased to a value less  
263 than 4  $\mu\text{g m}^{-3}$ , this grid should be regarded as “NO<sub>x</sub> titration”; (3) if  $\Delta O_{3V}$  decreased by more than 4  $\mu\text{g m}^{-3}$ ,  
264 with this reduction being twice as large as the  $\Delta O_{3N}$  reduction (or  $\Delta O_{3N}$  increase), this grid was likely  
265 controlled by VOCs; (4) if  $\Delta O_{3N}$  decreased by more than 4  $\mu\text{g m}^{-3}$ , with the reduction being twice as large  
266 as the  $\Delta O_{3V}$  reduction, this grid was likely controlled by NO<sub>x</sub>; (5) if  $\Delta O_{3N}$  and  $\Delta O_{3V}$  both decreased by more  
267 than 4  $\mu\text{g m}^{-3}$  and the ratio between them was less than 2:1 or 1:2, this grid was likely controlled by both  
268 NO<sub>x</sub> and VOCs. Details regarding the identification explained above can be found in Figure 7(f). The  
269 frequency of precursor control types in each grid in June was determined and is shown in Figure 8(a-e).  
270 The NO<sub>x</sub> titration scarcely appeared in the model domain. The frequency of the “no control” type entirely  
271 exceeded 50% over the background regions when the O<sub>3</sub> mass burden was lower than 120  $\mu\text{g m}^{-3}$  and



272 gradually decreased as the O<sub>3</sub> mass burden increased. Over the O<sub>3</sub> pollution areas, a grid with a “no  
273 control”-type frequency higher than 10% was seldom found. Specific to the considered regions, the urban  
274 area of Beijing, Tianjin, Tangshan, southern Hebei, and northern and western Shandong were mainly under  
275 VOC control, while the outer suburb of Beijing, all of Shanxi, and northern Hebei were mainly under NO<sub>x</sub>  
276 control. The “both control” type generally appeared in the transitional zone between NO<sub>x</sub> and VOC control.  
277 Compared with the results shown in Figures 6 and 7, the distribution feature of NO<sub>x</sub> and VOC contributions  
278 highly coincided with that of the O<sub>3</sub> precursor sensitivity types, which demonstrated that this method is  
279 reliable.

280 In addition to the contribution feature of emission sources estimated using the ISAM, the effect of  
281 reducing anthropogenic emissions on the O<sub>3</sub> mass burden was also necessary to learn because the formation  
282 of O<sub>3</sub> from NO<sub>x</sub> and VOC emissions is a typical nonlinear process. The brute-force method, which can  
283 realistically capture the nonlinear processes of secondary pollutant formation, was applied. Therefore,  
284 several sensitivity tests were designed, as shown in Table 3. First, the zero-out (100% source removal)  
285 simulations of four major sectors, i.e., industry, power plants, transport, and residential (sensitivity tests ZI,  
286 ZP, ZT, and ZR, respectively), were conducted to evaluate the efficiency of emission reduction for different  
287 sources in the NCP. Figure 9 presents the results of the brute-force sensitivity tests and the NO<sub>x</sub> and VOC  
288 emission flux of each major sector. The removal of the industry sector is shown to have been the most  
289 efficient way to decrease the O<sub>3</sub> mass burden, and the variation of 8H-O<sub>3</sub> between 20 and 30 μg m<sup>-3</sup> was  
290 generally concentrated in the high mass concentration regions. The main reason is likely that the VOC  
291 emission flux of the industry sector was significantly higher than that of the other sectors. Removal of the  
292 residential sector could also decrease the O<sub>3</sub> mass burden in most of the VOC control regions due to its  
293 VOC emission flux being notably higher than that of NO<sub>x</sub>. In contrast, removal of the transport and power  
294 plant sectors could not effectively reduce the O<sub>3</sub> mass burden and even increased the mass burden in high  
295 pollution areas, such as southern Beijing, Tianjin, Tangshan, southern Hebei, Jinan, and other parts of  
296 Shandong. The NO<sub>x</sub> emission flux of these two kinds of sectors was clearly higher than that of VOCs,  
297 especially for the power plant sector. It also caused the 8H-O<sub>3</sub> mass burden to decrease by 5-10 μg m<sup>-3</sup> in  
298 Shanxi as a result of the removal of the power plant sector. In summary, if we focus on the major pollution  
299 regions of the NCP, including Beijing, Tianjin, Hebei, and Shandong, reduction of the industry and  
300 residential emission sectors should be an effective way to control the O<sub>3</sub> mass burden during heavy O<sub>3</sub>  
301 pollution episodes.



302 In addition, the realistic pollution control strategies are supposed to be applied to a specific sector in  
303 the high emission regions (HERs) and used to develop a comprehensive reduction scheme; thus, a detailed  
304 analysis is necessary to investigate more accurate and practical strategies. Other than applying the simple  
305 zero-out sensitivity test over entire objective regions, we selected the regions that include cities and towns  
306 with high anthropogenic emission flux in the Beijing, Tianjin, Hebei, and Shandong (BTHS) region to more  
307 accurately match real emission control. Figure 10 presents the selected regions and the emission flux of  
308  $\text{NO}_x$  and VOCs from the industry sector, residential sector, and multiple combinations. First, the change in  
309 8H- $\text{O}_3$  mass concentration associated with the anthropogenic emission in selected regions (Figures 10(i)  
310 and 10(j)) was compared with that in the entire BTHS region (sensitivity tests A20%-HERs and A20%-  
311 BTHS), as shown in Figures 11(a) and 11(b), respectively. The distribution patterns of the 8H- $\text{O}_3$  mass  
312 burden variation were notably similar to each other, and the positive and negative values generally appeared  
313 in the same regions. However, the negative value in Figure 11(b) was clearly higher than that in Figure  
314 11(a). This disparity indicates that significant overestimation of the  $\text{O}_3$  mass burden variation might occur  
315 when we conduct a brute-force sensitivity test with broad reductions in emissions in the entire objective  
316 regions.

317 According to the results of the zero-out sensitivity tests, the industry and residential sectors were the  
318 major emission sources of  $\text{O}_3$ , while the power plant sector did not benefit  $\text{O}_3$  formation. Thus, the effects  
319 of reducing these industry and residential sectors were estimated using the brute-force method with 20%  
320 emission intensity in the selected regions of BTHS (Figures 10(a) and 10(b)). Figures 11(c) and 11(d) show  
321 the variation of  $\text{O}_3$  associated with the industry and residential emission sectors (sensitivity tests I20%-  
322 HER and R20%-HER), respectively. The 8H- $\text{O}_3$  mass concentration could decrease by 10-12  $\mu\text{g m}^{-3}$  in  
323 most of Shandong, especially in the strong polluted regions shown in Figure 11(c). In contrast, the value  
324 slightly increased in the urban areas of Shijiazhuang, Tianjin, and Tangshan. In Figure 5(f), the 8H- $\text{O}_3$  mass  
325 burden was relatively lower in these regions. Thus, the  $\text{O}_3$  mass burden can be decreased rapidly by  
326 controlling the industry emissions under a heavy  $\text{O}_3$  pollution background. Figure 11(d) shows that the 8H-  
327  $\text{O}_3$  mass concentration decreased overall in BTHS, though the range was only 1-5  $\mu\text{g m}^{-3}$ . The likely main  
328 reason is that the emission of VOCs was higher than that of  $\text{NO}_x$  from the residential sector, while the  
329 emission intensity from the residential sector was relatively lower than that from industry. The mass burden  
330 of  $\text{O}_3$  can also be reduced by controlling the residential emissions in the urban areas of Shijiazhuang, Tianjin,  
331 and Tangshan.



332 In addition, the influence of different combinations of emission sectors in BTHS was discussed.  
333 Figures 11(e) and 11(f) present the change in 8H-O<sub>3</sub> mass concentration associated with a 20% emission  
334 intensity for both the industry and residential sectors (sensitivity test IR20%-HERs) and the industry,  
335 transport, and residential sectors (sensitivity test ITR20%-HERs), respectively. The O<sub>3</sub> mass burden  
336 generally decreased sharply in BTHS, as shown in Figure 11(e), especially in the regions of Shandong with  
337 heavy pollution. The range and magnitude of decrease can obviously be enhanced while considering the  
338 reduction of the transport sector, as shown in Figure 11(f). Notably, the mass concentration of 8H-O<sub>3</sub> could  
339 decrease from 180-200 μg m<sup>-3</sup> to 160-180 μg m<sup>-3</sup> in the polluted regions of BTHS. Compared with the zero-  
340 out sensitivity test in Figure 9, the decrease in 8H-O<sub>3</sub> mass burden in Figure 11(f) was still clearly lower  
341 than that of ZI. This deviation indicates that the contribution source from other regions except BTHS should  
342 also be important. Even though 80% of the emission intensity was removed, the reduction in 8H-O<sub>3</sub> mass  
343 concentration still barely exceeded 20 μg m<sup>-3</sup> in the NCP, as shown in Figures 11(c), 11(d), and 11(e), which  
344 means that it was difficult to keep the O<sub>3</sub> mass burden under the Grade II standard by controlling only the  
345 industry and residential emission sectors in HERs.

346 Therefore, more brute-force sensitivity tests with HERs emissions varied from 50% to 0% were  
347 conducted. The regional average 8H-O<sub>3</sub> mass concentrations in Beijing, Tianjin, Shijiazhuang, Jinan, and  
348 Tangshan with changes in emission are shown in Figure 12. Three series of sensitivity tests were conducted:  
349 reduction of the IR (industry and residential), ITR (industry, transport, and residential) and All (industry,  
350 transport, power plant, and residential) emission sectors. As shown, the 8H-O<sub>3</sub> mass concentration was  
351 higher than 160 μg m<sup>-3</sup> in all five cities, while the emission percentage was 100%. When the emissions  
352 reduced to 50%, the 8H-O<sub>3</sub> mass concentrations of these three series slightly decreased for Beijing, Tianjin,  
353 Tangshan, and Jinan but increased for Shijiazhuang. The decrease in 8H-O<sub>3</sub> mass concentration as a result  
354 of reducing the IR emission was similar to that of the ITR emission when the emissions were reduced from  
355 50% to 40% for all five cities but was not significant when the reduction was less than 40%. The lines  
356 corresponding to the ITR and All emission sectors generally decreased coherently for these five cities when  
357 the emissions were reduced from 50% to 30%. However, the effect of the ITR reduction was obviously  
358 weaker than that of the All reduction when the reduction was less than 30%. The decrease in 8H-O<sub>3</sub> mass  
359 burden exceeded 12 μg m<sup>-3</sup> when the All emission reduction was least, and the air quality in all five of these  
360 cities could reach the Grade II standard. This phenomenon indicated that the influence of the transport and  
361 power plant emission sectors on the decrease in O<sub>3</sub> mainly occurred after removing 60% of the IR or 70%



362 of the ITR emission intensity, respectively. Thus, an emission control sequence for different sectors should  
363 be considered when exploring more effective strategies.

364

## 365 **5. Conclusions**

366 In this study, an air quality modeling system referred to as RAMS-CMAQ was applied to simulate the  
367 O<sub>3</sub> mass concentration, and several sensitivity tests were conducted to investigate the O<sub>3</sub> pollution and to  
368 discuss the relationship between O<sub>3</sub> production and emission contributions over the NCP in January and  
369 June of 2015. First, the modeled daily meteorological factors (temperature, relative humidity, and wind  
370 field) and hourly mass concentrations of O<sub>3</sub> and its precursor NO<sub>2</sub> were compared with ground-based  
371 observation data to evaluate the accuracy and reliability. The simulation results were generally good and  
372 able to broadly capture the values and variation trend of the observation data. Focusing on the heavy O<sub>3</sub>  
373 pollution period in June, an advanced source apportionment tool called ISAM was coupled with RAMS-  
374 CMAQ and applied to estimate the regional transport contributions, with individual tracers for nitrogen and  
375 VOC species used to represent the O<sub>3</sub> chemical formation regime attributed to either NO<sub>x</sub> or VOC emission  
376 sources in the NCP. Then, a unique method that is suitable for three-dimensional chemistry/transport models  
377 was used to distinguish the O<sub>3</sub>-NO<sub>x</sub>-VOC sensitivity features and identify the precursor sensitivity in each  
378 grid of the model domain. Therefore, the O<sub>3</sub> mass burden sensitivities to NO<sub>x</sub> and VOC emission changes  
379 and the correlative regional transport contribution features among major anthropogenic source regions in  
380 the NCP can be clearly investigated using these methods. In addition, several brute-force sensitivity tests  
381 were conducted to discuss the role of the main anthropogenic emission sectors on reducing the O<sub>3</sub> mass  
382 burden, and an attempt was made to provide valuable suggestions for exploring more effective strategies  
383 for preventing O<sub>3</sub> pollution. The results are summarized as follows:

384 1. The simulation results show that the seasonal variation of O<sub>3</sub> was significant and that the heavy  
385 mass burden of 8H-O<sub>3</sub>, which exceeded the Grade II standard, generally occurred in southern Beijing, Hebei  
386 and almost all of Tianjin and Shandong in June. The mass burden of 8H-O<sub>3</sub> reached 180-200 μg m<sup>-3</sup> mainly  
387 in the tri-province area of Hebei, Shandong, and Henan. The distribution pattern and seasonal variation of  
388 8H-O<sub>3</sub> were obviously different from those of its precursors, which indicates that the formation and  
389 transport processes of O<sub>3</sub> should be complex in the NCP.

390 2. The results of RAMS-CMAQ-ISAM show that the emission sources in Shandong and Hebei were  
391 the major contributors to O<sub>3</sub> production in the NCP. In addition to these two provinces, the O<sub>3</sub> mass burden



392 in Beijing and Tianjin was also significant. The emissions from Hebei and Shandong contributed 15-20%  
393 and 5-10% to Beijing and 10-20% and 15-20% to Tianjin, respectively. However, the O<sub>3</sub> mass burden in  
394 these two provinces was generally contributed by the provinces themselves. The results also show that the  
395 contribution of VS was clearly higher than that of NS in Beijing, Tianjin, Hebei, and Shandong, which  
396 indicates that the O<sub>3</sub> mainly originated from VOC emission sources. On the other hand, the emission sources  
397 in the Shanxi province almost had no impact on the O<sub>3</sub> mass burden in other regions of the NCP due to the  
398 hinderance to pollutant transport provided by the Taihang Mountains.

399 3. The results of identification of the O<sub>3</sub>-NO<sub>x</sub>-VOC sensitivity feature show that the VOC control  
400 mainly occurred over all of Tianjin and Tangshan and southern Beijing (urban area) and Hebei, where the  
401 O<sub>3</sub> mass concentration reached 160-180 μg m<sup>-3</sup>. The north central part of Shandong and urban area of Jinan  
402 were also mainly under the VOC control. The frequencies of VOC control and the "both control" type was  
403 generally equal in the region of Hebei and Shandong where the O<sub>3</sub> mass concentration reached 180-200 μg  
404 m<sup>-3</sup>. The NO<sub>x</sub> control generally appeared in the regions of the NCP where the O<sub>3</sub> mass concentration reached  
405 120-160 μg m<sup>-3</sup>. In the major cities with O<sub>3</sub> pollution, including Beijing, Tianjin, Shijiazhuang, and Jinan,  
406 the O<sub>3</sub>-NO<sub>x</sub>-VOC sensitivity feature was the same: VOC control dominated the urban area, while "both  
407 control" and NO<sub>x</sub> control dominated the suburban and remote areas, respectively.

408 4. The results of the zero-out sensitivity tests show that the IR emission sectors were two important  
409 contributors to ozone formation, as they were the major sources of VOCs, while the power plant emission  
410 sector did not benefit O<sub>3</sub> pollution control in the high mass burden regions due to the greater emission of  
411 NO<sub>x</sub> versus VOCs.

412 On the other hand, the results of the brute-force sensitivity tests show that the effects of IR, ITR, and  
413 All emission control on the decrease in O<sub>3</sub> were similar when their reduction percentages were higher than  
414 40%. Meanwhile, the effects of ITR and All emission control were similar while the reduction percentages  
415 were higher than 30%. When the reduction percentage dropped below 30%, the nonlinearity of O<sub>3</sub>  
416 formation was notable, and the power plant sector could make significant contributions to the decrease in  
417 O<sub>3</sub>. Thus, the control strategies should be promptly adjusted based on the emission reduction, and the  
418 emission sector combination should be precisely chosen to achieve better efficiency. The modeling system  
419 allows us to capture valuable information regarding how to choose the correct sequence and efficient  
420 combinations by exploring the key thresholds from the bulk of sensitivity tests regarding crucial parameters.

421



422

423 **References**

- 424 Benkovitz, C. M., Schultz, M.T., Pacyna, J., Tarrason, L., Dignon, J., Voldner, E.C., Spiro, P.A., Logan, A.,  
425 and Graedel, T.E.: Global gridded inventories of anthropogenic emissions of sulfur and nitrogen, *J.*  
426 *Geophys. Res.*, 101(29), 239-253, 1996.
- 427 Castell, N., Stein, A., Mantilla, E., Salvador, R., and Millan, M.: Evaluation of the use of photochemical  
428 indicators to assess ozone-NO<sub>x</sub>-VOC sensitivity in the Southwestern Iberian Peninsula, *J. Atmos.*  
429 *Chem.*, 63(1), 73-91, 2009.
- 430 Cotton, W. R., Pielke, R. A., Walko, R. L., Liston, G. E., Tremback, C. J., Jiang, H., McAnelly, R. L.,  
431 Harrington, J. Y., Nicholls, M. E., Carrio, G. G., and McFadden, J. P.: RAMS 2001: current status  
432 and futures directions, *Meteor. Atmos. Phys.*, 82, doi:10.1007/s00703-001-0584-9, 2003.
- 433 Deng, X., Zhou, X., Wu, D., Tie, X., Tan, H., Li, F., Bi, X., Deng, T., and Jiang, D.: Effect of atmospheric  
434 aerosol on surface ozone variation over the Pearl River Delta region, *Sci. China Earth Sci.*, 54(5),  
435 744-752, 2011.
- 436 Dufour, G., Fremenko, M., Orphai, J., and Flaud, J.: IASI observations of seasonal and day-to-day  
437 variations of tropospheric ozone over three highly populated areas of China: Beijing, Shanghai, and  
438 Hong Kong, *Atmos. Chem. Phys.*, 10, 3787-3801, 2010.
- 439 Gao, W., Tang, G., Ji, D., and Wang, Y.: Implementation effects and countermeasures of China's air  
440 pollution prevention and control action plan, *Res. Environ. Sci.*, 29(11), 1567-1574, 2016. (In  
441 Chinese)
- 442 Han, X., Zhang, M., Gao, J., Wang, S., Chai, F.: Modeling analysis of the seasonal characteristics of haze  
443 formation in Beijing, *Atmos. Chem. Phys.*, 14, 10231-10248, 2014.
- 444 Han, X., Zhang, M., Zhu, L., Skorokhod, A.: Assessment of the impact of emissions reductions on air  
445 quality over North China Plain, 7, 249-259, 2016.
- 446 Kleinman, L. I., Daum, P. H., Lee, Y. N., Nunnermacker, L. J., Springston, S. R., Lloyd, J., and Rudolph,  
447 J.: Ozone production efficiency in an urban area, *J. Geophys. Res.*, 107, D23, 23, 2002.
- 448 Kwok, R. H. F., Baker, K. R., Napelenok, S. L., and Tonnesen, G. S.: Photochemical grid model  
449 implementation and application of VOC, NO<sub>x</sub>, and O<sub>3</sub> source apportionment, *Geosci. Model Dev.*,  
450 7(5), 99-114, 2014.
- 451 Kwok, R., Napelenok, S., and Baker, K.: Implementation and evaluation of PM<sub>2.5</sub> source contribution  
452 analysis in a photochemical model, *Atmos. Environ.*, 80, 398-407, 2013.
- 453 Li, H., Zhang, Q., Chen, C., Wang, L., Wei, Z., Zhou, S., Parworth, C., Zheng, B., Canonaco, F., Prevot, A.,  
454 Chen, P., Zhang, H., and He, K.: Wintertime aerosol chemistry and haze evolution in an extremely  
455 polluted city of North China Plain: significant contribution from coal and biomass combustions,  
456 *Atmos. Chem. Phys.*, 17, 4751-4768, 2017.
- 457 Li, M., Zhang, Q., Kurokawa, J., Woo, H., He, K., Lu, Z., Ohara, T., Song, Y., Streets, D., Carmichael, G.,  
458 Cheng, Y., Huo, H., Liu, F., Su, H., and Zhang, B.: MIX: a mosaic Asian anthropogenic emission  
459 inventory for the MICS-Asia and the HTAP projects, *Atmos. Chem. Phys. Discuss.*, 15, 34813-34869,  
460 2015.
- 461 Lin, W., Xu, X., Zhang, X., and Tang, J.: Contributions of pollutants from North China Plain to surface  
462 ozone at the Shangdianzi GAW Station, *Atmos. Chem. Phys.*, 8, 5889-5898, 2008.
- 463 Liu, X., Zhang, Y., Xing, J., Zhang, Q., Wang, K., Streets, D., Jang, C., Wang, W., and Hao, J.:  
464 Understanding of regional air pollution over China using CMAQ, part II. Process analysis and





- 465 sensitivity of ozone and particulate matter to precursor emissions, *Atmos. Environ.*, 44, 3719-3727,  
466 2010.
- 467 Nenes, A., Pilinis, C., and Pandis, S.N.: Continued development and testing of a new thermodynamic  
468 aerosol module for urban and regional air quality models, *Atmos. Environ.*, 33, 1553-1560, 1999.
- 469 Nie, T., Li, X., Wang, X., Shao, M., and Zhang, Y.: Characteristics of the Spatial Distributions of Ozone-  
470 Precursor Sensitivity Regimes in Summer over Beijing, *Acta Scientiarum Naturalium Universitatis  
471 Pekinensis*, 50(3), 557-564, 2014. (in Chinese)
- 472 Olivier, J., Bouwman, A., Maas, C., and Berdowski, J.: Emission database for global atmospheric research,  
473 *Environ. Monit. Assess.*, 31, 93-106., 1994.
- 474 Ran, L., Zhao, C., Xu, W., Han, M., Lu, X., Han, S., Lin, W., Xu, X., Gao, W., Yu, Q., Geng, F., Ma, N.,  
475 Deng, Z., and Chen, J.: Ozone production in summer in the megacities of Tianjin and Shanghai,  
476 China: a comparative study, *Atmos. Chem. Phys.*, 12, 7531-7542, 2012.
- 477 Sarwar, G., Luecken, D., Yarwood, G., Whitten, G. Z., Carter, W. P. L.: Impact of an updated carbon bond  
478 mechanism on predictions from the CMAQ modeling system: preliminary assessment, *J. Appl.  
479 Meteor. Climatol.*, 47, 3-14, 2008.
- 480 Sillman, S. and West, J.: Reactive nitrogen in Mexico City and its relation to ozone-precursor sensitivity:  
481 results from photochemical models, *Atmos. Chem. Phys.*, 9, 3477-3489, 2009.
- 482 Streets, D., Bond, T., Carmichael, G., Fernandes, S., Fu, Q., He, D., Klimont, Z., Nelson, S. M., Tsai, N. Y.,  
483 Wang, : An inventory of gaseous and primary aerosol emissions in Asia in the year 2000, *J. Geophys.  
484 Res.*, 108, DOI: 10.1029/2002JD003093, 2003.
- 485 Tang, G., Wang, Y., Li, X., Ji, D., Hsu, S., Gao, X.: Spatial-temporal variations in surface ozone in Northern  
486 China as observed during 2009–2010 and possible implications for future air quality control  
487 strategies, *Atmos. Chem. Phys.*, 12, 2757-2776, 2012.
- 488 Tang, G., Zhu, X., Xin, J., Hu, B., Tao, S., Sun, Y., Zhang, J., Wang, L., Cheng, M., Chao, N., Kong, L., Li,  
489 X., and Wang, Y.: Modelling study of boundary-layer ozone over northern China - Part I: Ozone  
490 budget in summer, *Atmos. Res.*, 187, 128-137, 2017.
- 491 Tao, M., Chen, L., Su, L., and Tao, J.: Satellite observation of regional haze pollution over the North China  
492 Plain, *J. Geophys. Res.*, 117, D12203, doi:10.1029/2012JD017915, 2012.
- 493 van der Werf, G. R., Randerson, J. T., Giglio, L., Collatz, G. J., Mu, M., Kasibhatla, P. S., Morton, D. C.,  
494 DeFries, R. S., Jin, Y., van Leeuwen, T. T.: Global fire emissions and the contribution of deforestation,  
495 savanna, forest, agricultural, and peat fires (1997-2009), *Atmos. Chem. Phys.*, 10, 11707-11735, 2010.
- 496 Wang, X., Sun, M., Yang, T., and Wang, Z.: Interdecadal change in frequency of dust-haze episodes in  
497 North China Plain, *Clim. Environ. Res.*, 18, 165–170, 2013 (in Chinese).
- 498 Wang, Y., Konopka, P., Liu, Y., Chen, H., Muller, R., Ploger, F., Riese, M., Cai, Z., and Lu, D.: Tropospheric  
499 ozone trend over Beijing from 2002–2010: ozonesonde measurements and modeling analysis, *Atmos.  
500 Chem. Phys.*, 12, 8389-8399, 2010.
- 501 Wang, Z. S., Chien, C. J., Tonnesen, G. S.: Development of a tagged species source apportionment  
502 algorithm to characterize three-dimensional transport and transformation of precursors and secondary  
503 pollutants, *J. Geophys. Res.*, 114, D21. DOI: 10.1029/2008JD010846, 2009.
- 504 Wu, R. and Xie, S.: Spatial Distribution of Ozone Formation in China Derived from Emissions of Speciated  
505 Volatile Organic Compounds, *Environ. Sci. Technol.*, 51(5), 2574-2583, 2017.
- 506 Xing, J., Wang, S., Zhu, Y.: Nonlinear response of ozone to precursor emission Changes in China: A  
507 modeling study using response surface methodology, *Atmos. Chem. Phys.*, 11(10):5027-5044, 2010.
- 508 Yang, Y., Wilkinson, J., and Russell, A.: Fast, direct sensitivity analysis of multi-dimensional





509 photochemical models, *Environ. Sci. Technol.*, 31(10), 2859–2868, 1997.

510 Yu, S. C., Eder, B., Dennis, R., Chu, S. H., and Schwartz, S.: New unbiased symmetric metrics for  
511 evaluation of air quality models, *Atmos. Sci. Lett.*, 7, 26–34, 2006.

512 Yu, S., Mathur, R., Sarwar, G., Kang, D., Tong, D., Pouliot, G. and Pleim, J.: Eta-CMAQ air quality  
513 forecasts for O<sub>3</sub> and related species using three different photochemical mechanisms (CB4, CB05,  
514 SAPRC-99): comparisons with measurements during the 2004 ICARTT study, *Atmos. Chem. Phys.*,  
515 10, 3001–3025, 2010.

516 Zhang, M., Uno, I., Zhang, R., Han, Z., Wang, Z., and Pu, Y.: Evaluation of the Models-3 Community  
517 Multi-scale Air Quality (CMAQ) modeling system with observations obtained during the TRACE-P  
518 experiment: comparison of ozone and its related species, *Atmos. Environ.*, 40, 4874-4882, 2006.

519 Zhou, S., Yang, L., Gao, R., Wang, X., Gao, X., Nie, W., Xu, P., Zhang, Q., and Wang, W.: A comparison  
520 study of carbonaceous aerosols in a typical North China Plain urban atmosphere: Seasonal variability,  
521 sources and implications to haze formation, *Atmos. Environ.*, 149, 95-103, 2017.

522

523

524

525

526

527

528

529

530

531

532

533

534

535

536

537

538

539

540

541

542

543

544

545

546

547

548

549

550

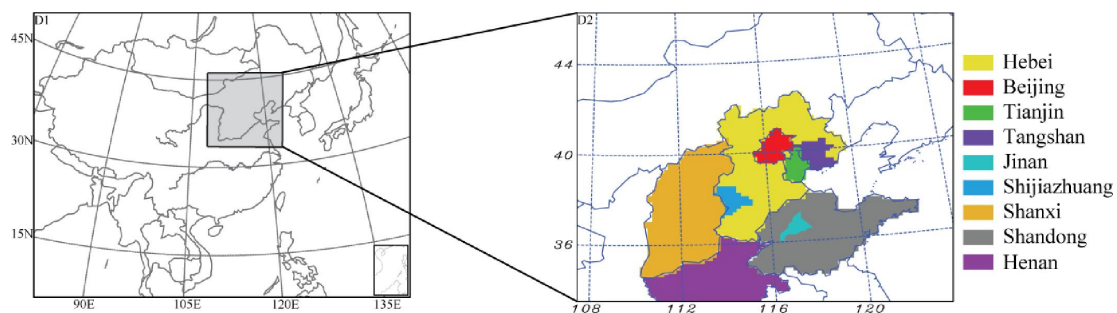
551

552



553

554



555

Figure 1 The model domain of this study, and the geographic locations of Beijing, Tianjin, Tangshan, Hebei, Shijiazhuang, Shanxi, Shandong, Jinan, and Henan.

556

557

558

559

560

561

562

563

564

565

566

567

568

569

570

571

572

573

574

575

576

577

578

579

580

581

582

583

584

585

586

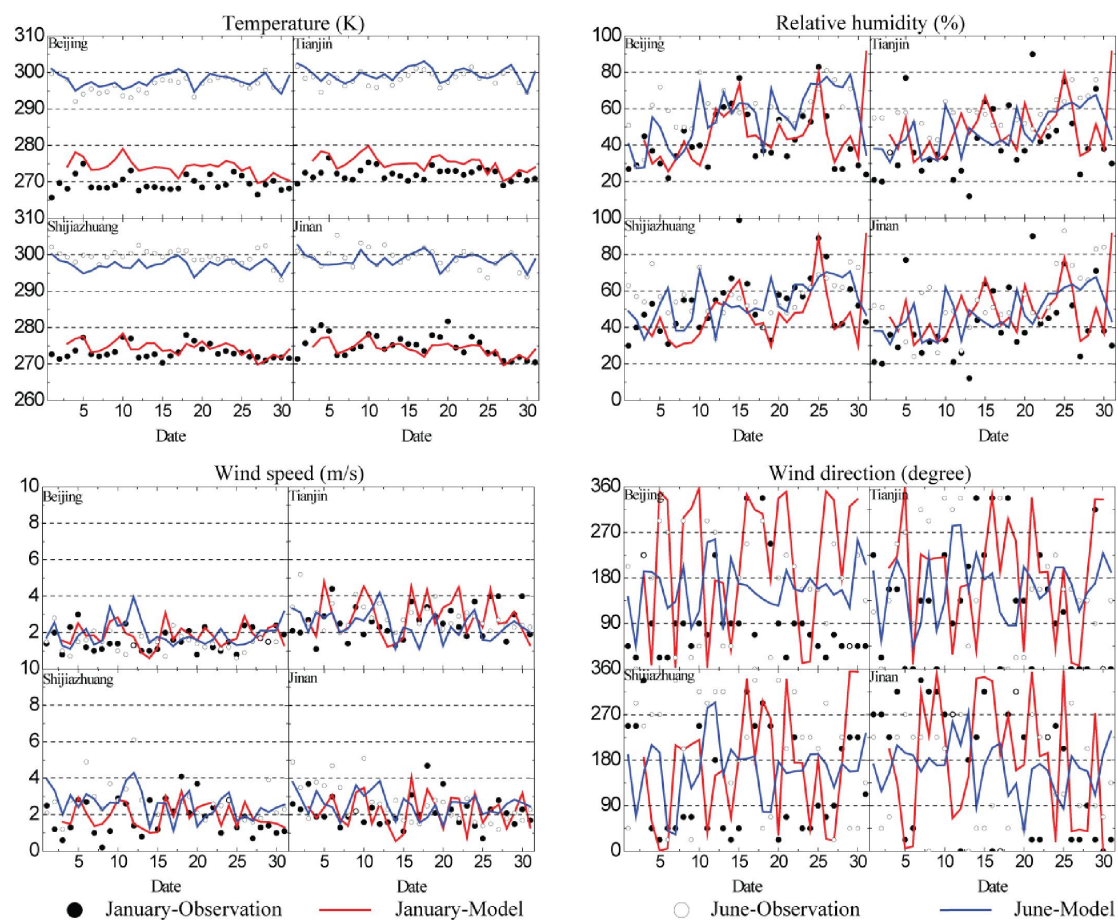
587

588



589

590



591

592 Figure 2. Observed and modeled daily average temperatures (K), relative humidity (%), wind speed (m/s), and maximum

593

594

595

596

597

598

599

600

601

602

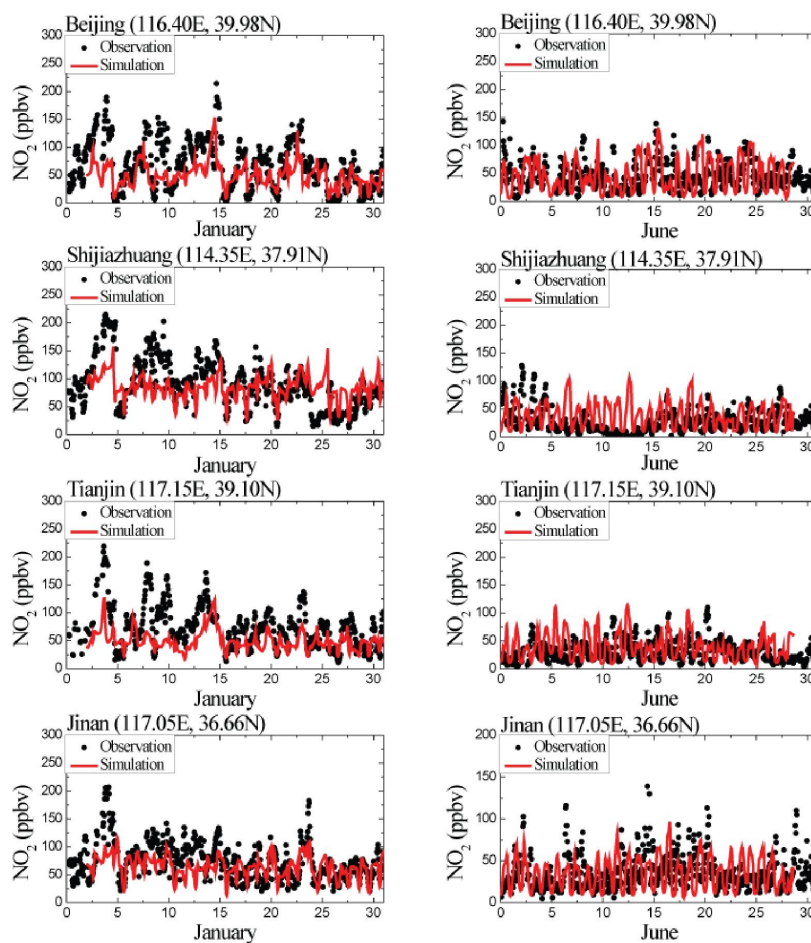
603

604

605

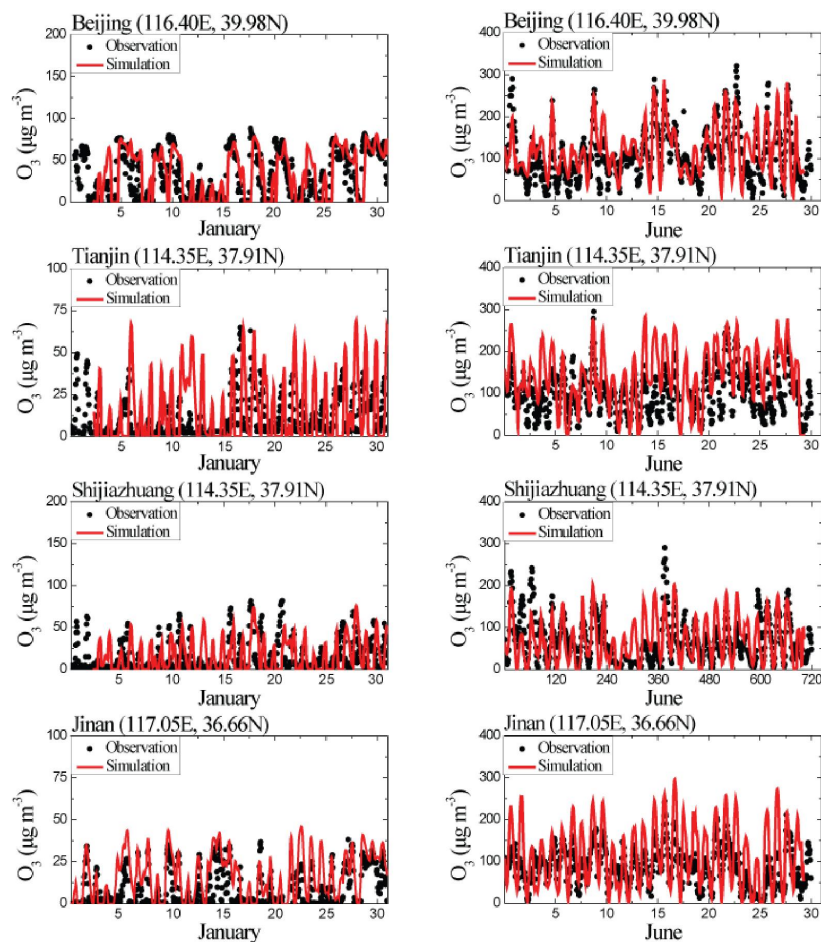


606  
607



608  
609  
610  
611  
612  
613  
614  
615  
616  
617  
618  
619  
620  
621  
622

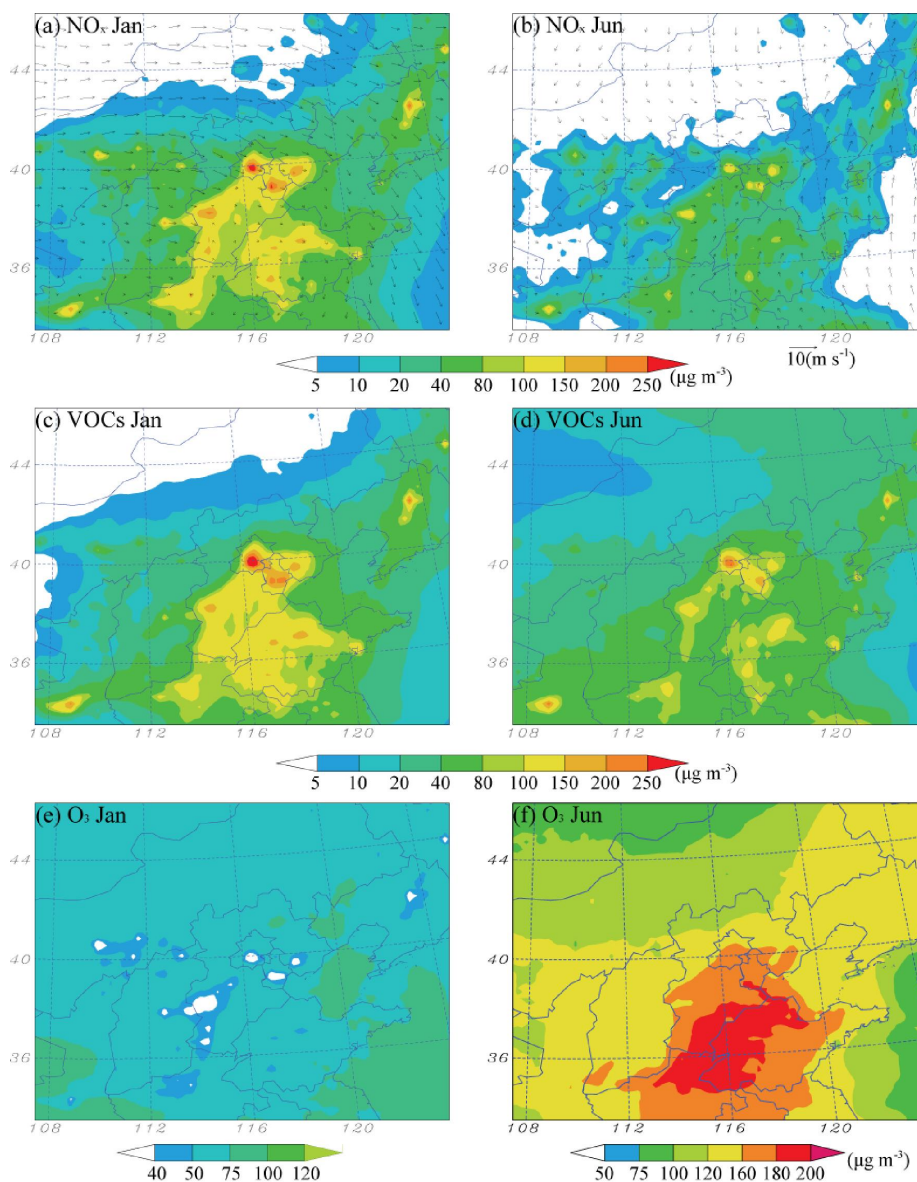
Figure 3. Observed (black circles) and modeled (red solid lines) hourly mass concentrations ( $\mu\text{g m}^{-3}$ ) of  $\text{NO}_2$  at Beijing, Shijiazhuang, Tianjin, and Jinan in January and June 2015.



623  
624  
625  
626  
627  
628  
629  
630  
631  
632  
633  
634  
635  
636  
637  
638  
639

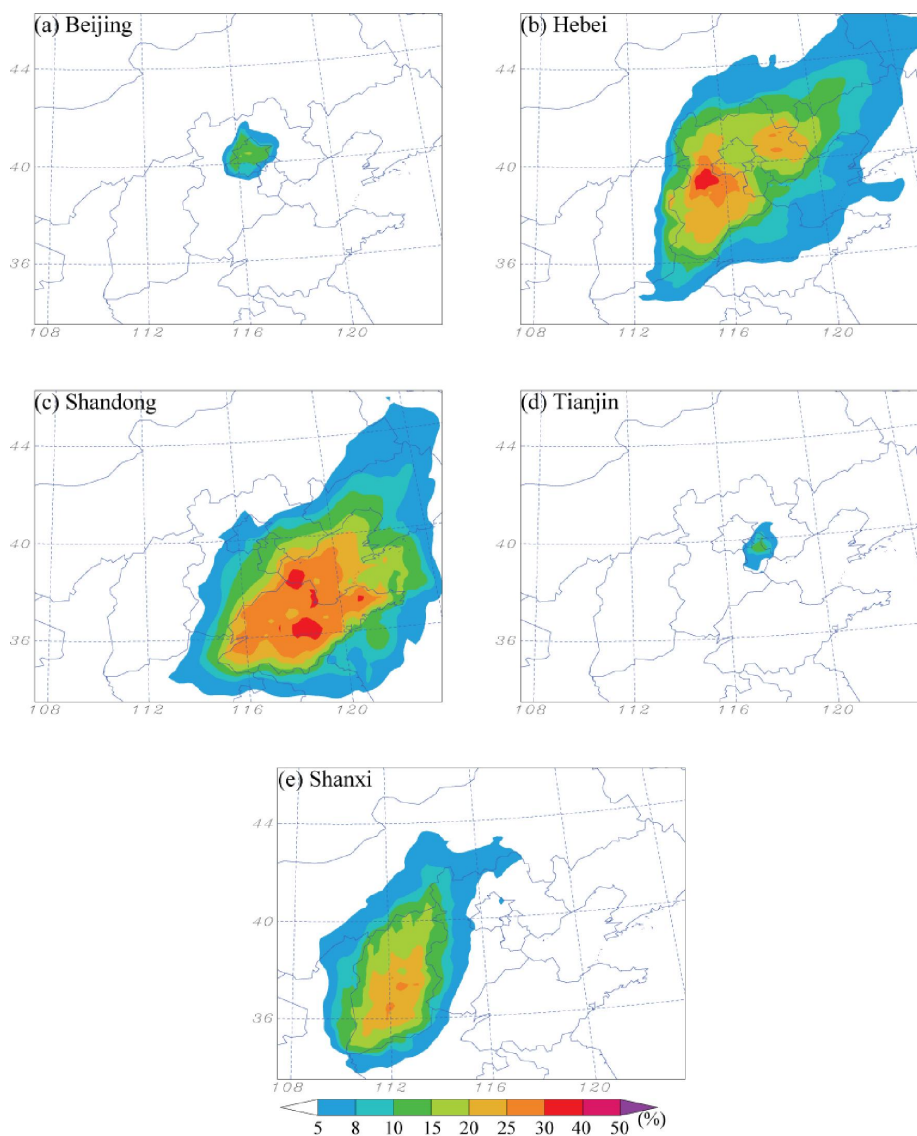
Figure 4. Observed (black circles) and modeled (red solid lines) hourly mass concentrations ( $\mu\text{g m}^{-3}$ ) of  $\text{O}_3$  at Beijing, Shijiazhuang, Tianjin, and Jinan in January and June 2015.





640  
641  
642  
643  
644  
645  
646  
647  
648  
649

Figure 5. The surface spatial distributions of monthly average  $\text{NO}_x$  (a-b) and VOCs (c-d), and maximum daily 8H- $\text{O}_3$  (e-f) in January and June 2015.



650  
651  
652  
653  
654  
655  
656  
657  
658  
659  
660

Figure 6. The regional contribution of NO<sub>x</sub>-sensitive O<sub>3</sub> from (a) Beijing, (b) Hebei, (c) Shandong, (d) Tianjin, and (e) Shanxi in June 2015.

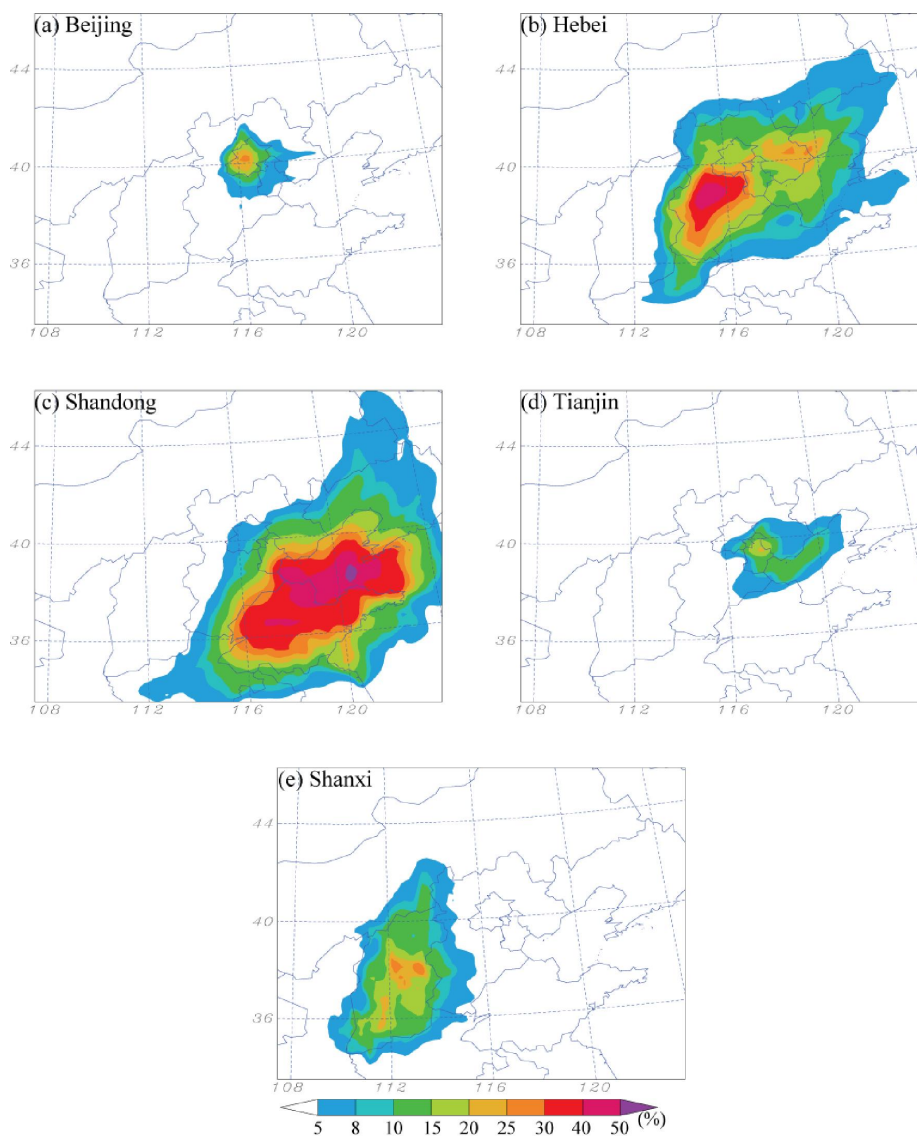


Figure 7. Same as Figure 5 but for VOC-sensitive O<sub>3</sub>.

661  
662  
663  
664  
665  
666  
667  
668  
669  
670  
671



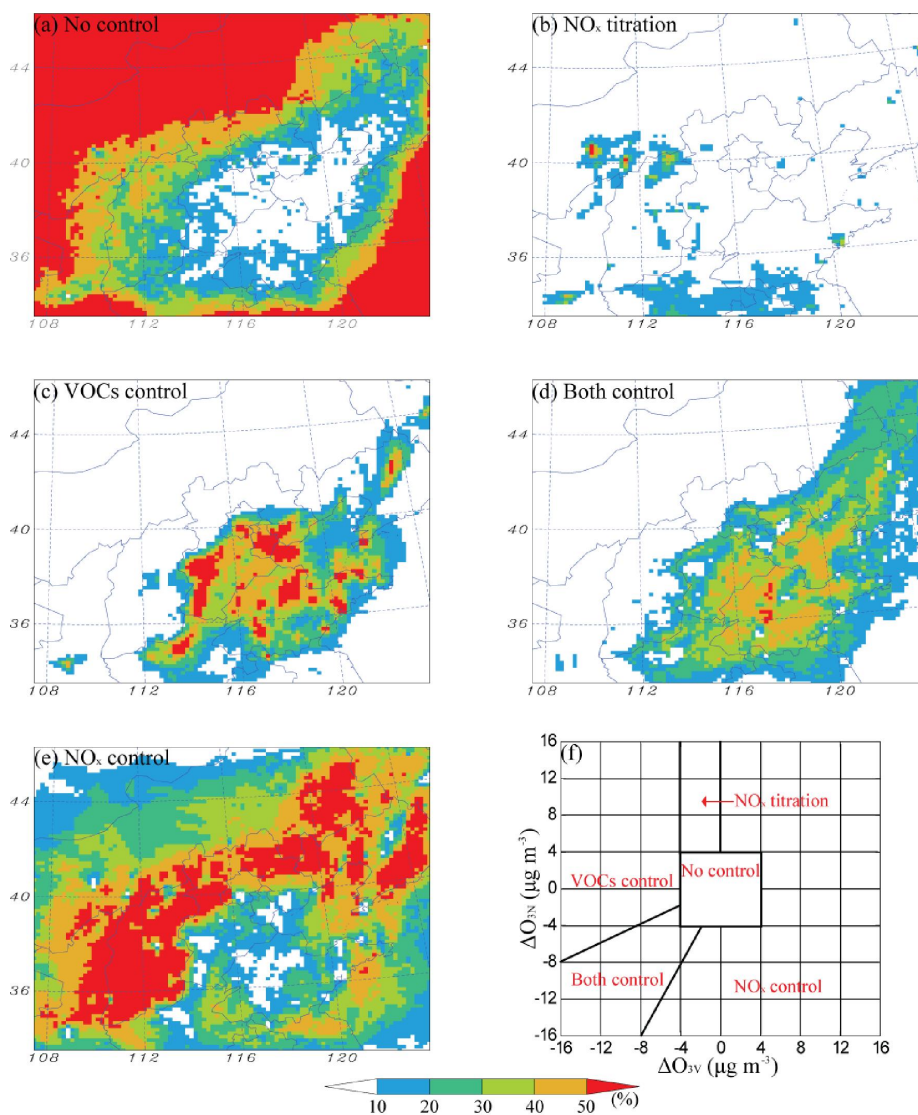
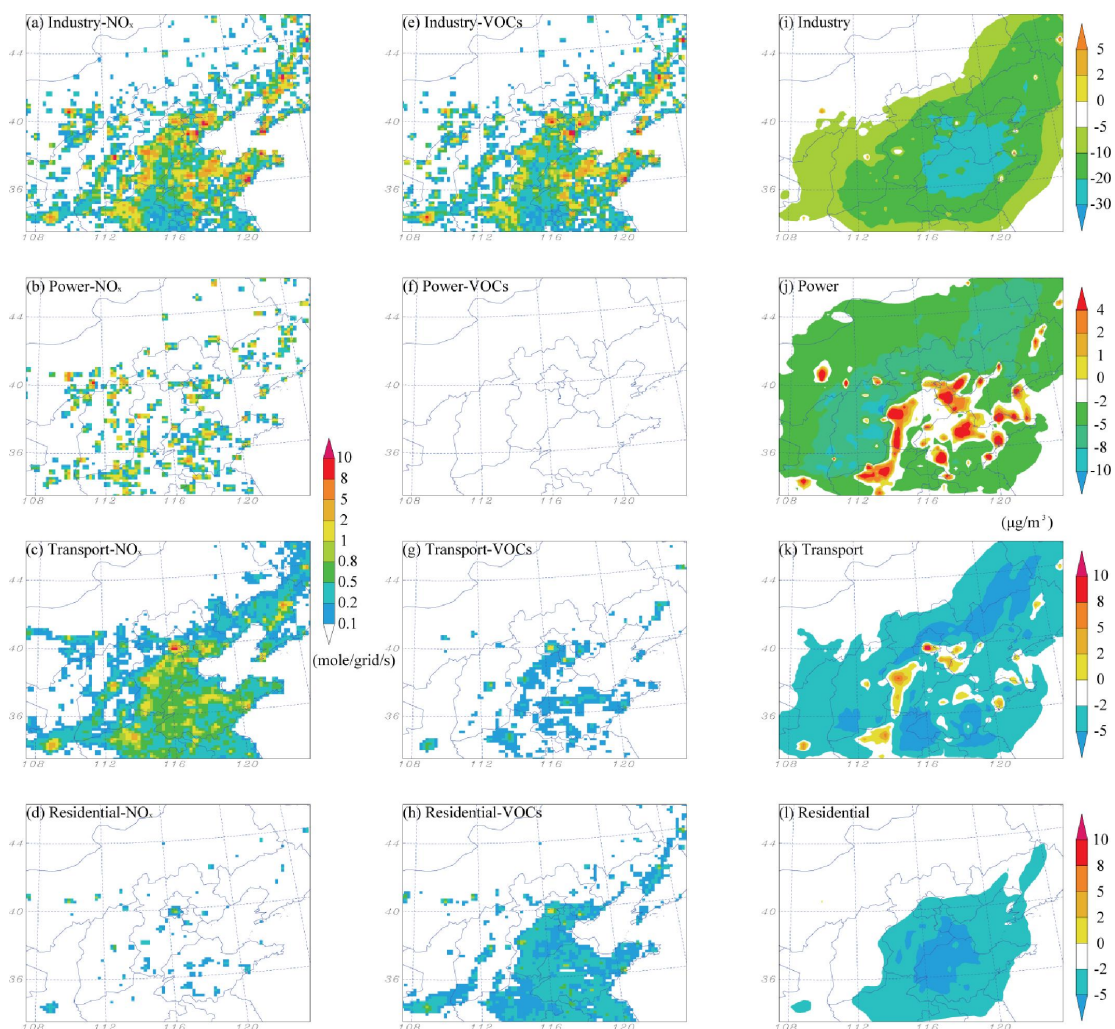


Figure 8. Distributions of the frequency of 8-hour ozone precursor sensitivity regions in June 2015.

672  
673  
674  
675  
676  
677  
678  
679  
680  
681  
682  
683



684

685

686

687

688

689

690

691

692

693

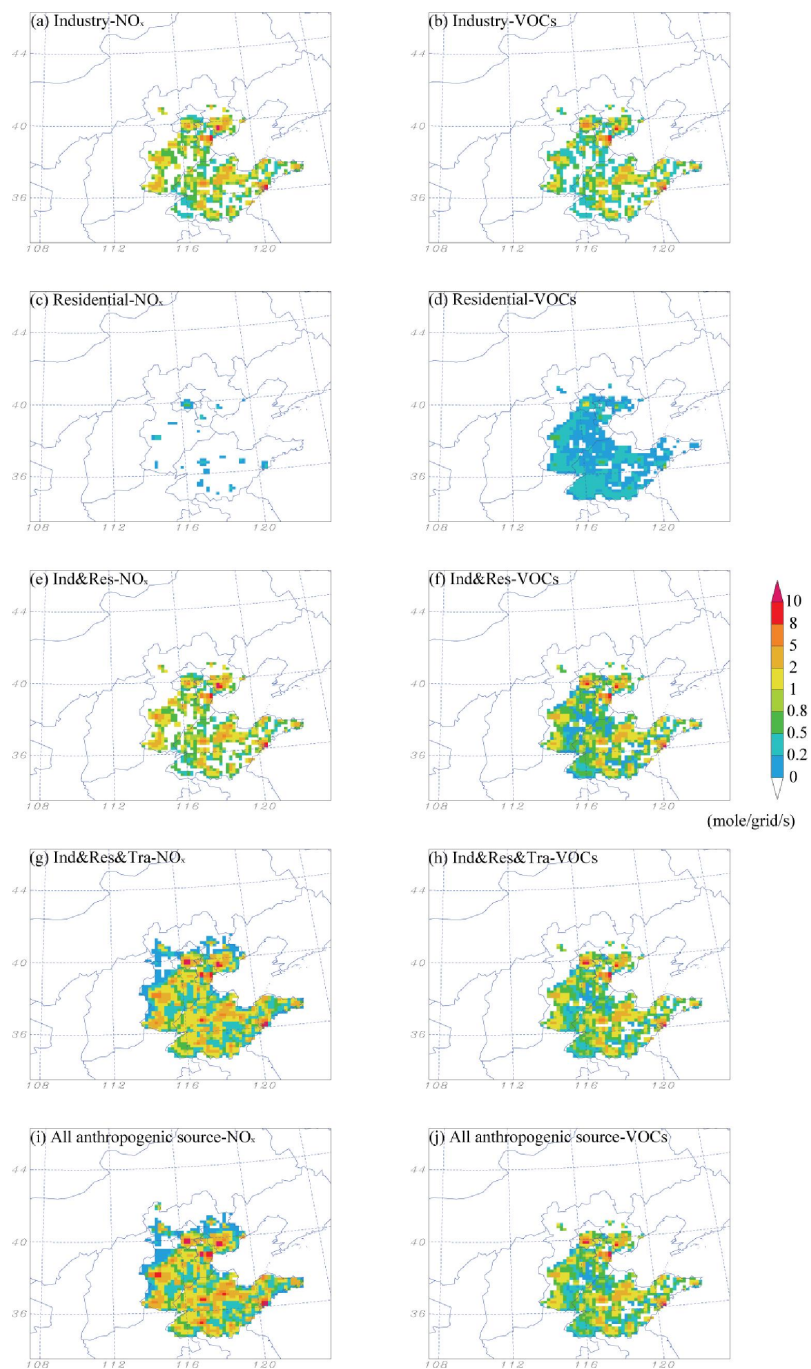
694

695

696

697

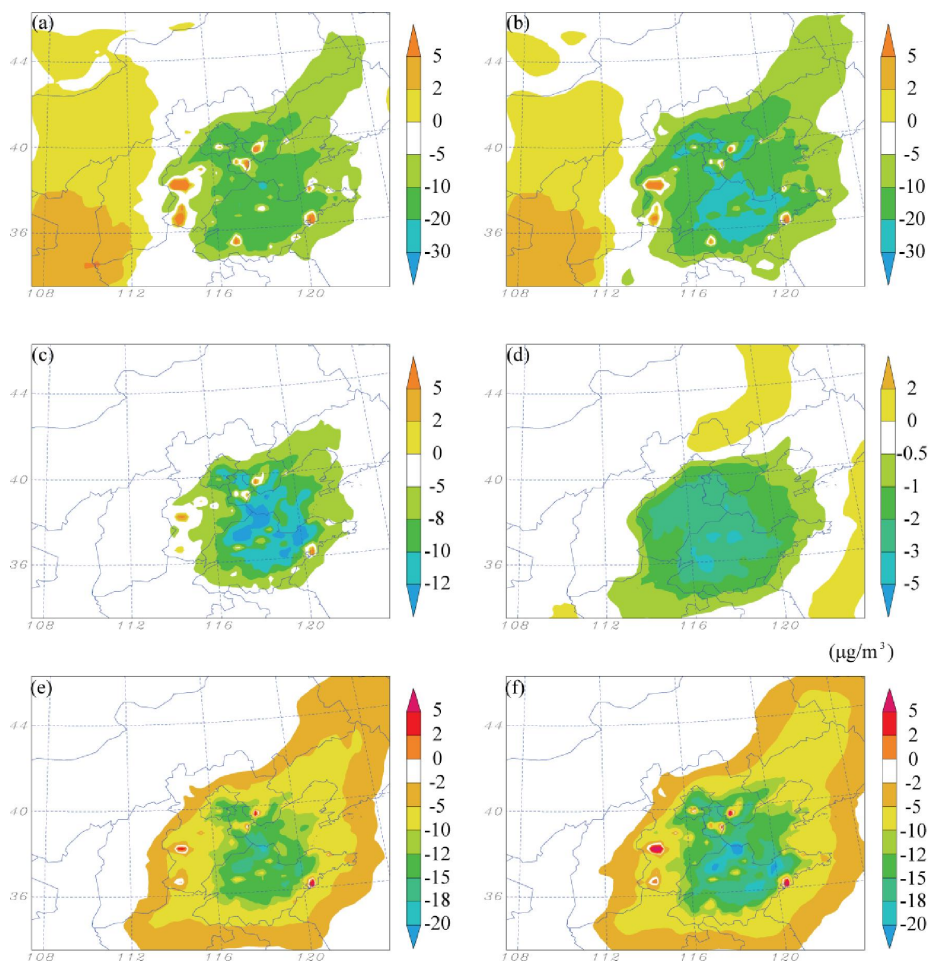
Figure 9. Distributions of the emission flux of  $\text{NO}_x$  and VOCs and the variation of mass concentration of  $8\text{H-O}_3$  associated with the ZI, ZP, ZT, and ZR in June.



698

699 Figure 10. Distributions of the NO<sub>x</sub> and VOCs emission flux from different sectors or combinations in the high emission  
700 regions of Beijing, Tianjin, Hebei, Shandong in June.

701



702

703

704

705

706

707

708

709

710

711

712

713

714

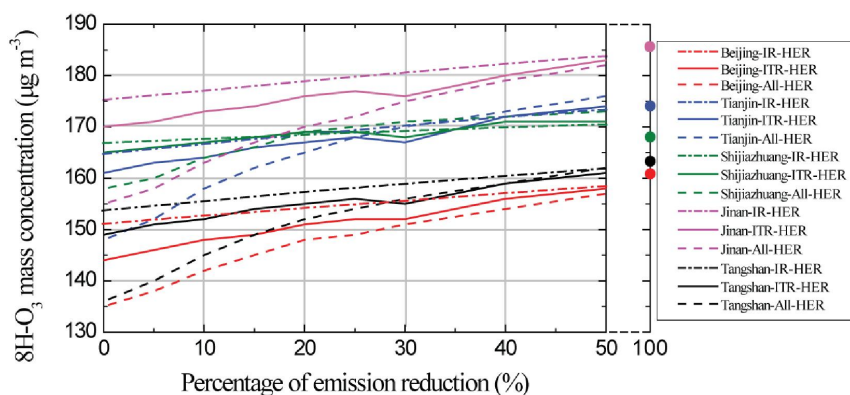
715

716

717

Figure 11. Distributions of the variation of 8H-O<sub>3</sub> mass concentration associated with brute force sensitivity tests: (a) A20%-HER; (b) A20%-BHTS; (c) I20%-HER; (d) R20%-HER; (e) IR20%-HER; (f) ITR20%-HER.





718

719

Figure 12. The variation of regional average 8H-O<sub>3</sub> mass concentrations in Beijing, Tianjin, Shijiazhuang, Jinan, and Tangshan with reduction of IR, ITR and All emissions, respectively.

720

721

722

723

724

725

726

727

728

729

730

731

732

733

734

735

736

737

738

739

740

741

742

743

744

745

746

747

748

749

750

751 Table 1. Statistical summary of the comparisons of the hourly NO<sub>2</sub> comparison between simulation and observation

		$N^a$	$C_{obs}^b$	$C_{mod}^c$	$\sigma_{obs}^d$	$\sigma_{mod}^e$	$R^f$	
NO <sub>2</sub>	Beijing	Jan	602	68.71	50.62	42.98	21.7	0.59
		Jun	588	45.39	46.75	24.95	28.49	0.53
	Jinan	Jan	616	74.39	63.26	33.98	19.55	0.55
		Jun	639	34.27	34.93	19.57	18.76	0.47
	Shijiazhuang	Jan	618	90.04	83.78	44.91	21.55	0.54
		Jun	629	26.11	38.82	21.59	22.26	0.44
	Tianjin	Jan	584	73.73	49.07	37.94	18.52	0.55
		Jun	639	30.02	40.29	18.36	23.25	0.52

752 <sup>a</sup> Number of samples753 <sup>b</sup> Total mean of observation754 <sup>c</sup> Total mean of simulation755 <sup>d</sup> Standard deviation of observation756 <sup>e</sup> Standard deviation of simulation757 <sup>f</sup> Correlation coefficient between daily observation and simulation

758

759

760

761

762

763

764

765

766

767

768

769

770

771

772

773

774

775

776

777

778

779

780

781

782

783

784

785

786 Table 2. Statistical summary of the comparisons of the hourly O<sub>3</sub> comparison between simulation and observation

		<i>N</i>	<i>C<sub>obs</sub></i>	<i>C<sub>mod</sub></i>	<i>σ<sub>obs</sub></i>	<i>σ<sub>mod</sub></i>	<i>R</i>	
O <sub>3</sub>	Beijing	Jan	615	33.57	37.88	27.58	27.2	0.54
		Jun	676	106.96	120.85	63.75	57.33	0.74
	Jinan	Jan	673	11.09	13.58	10.75	13.08	0.74
		Jun	693	87.91	111.44	45.54	71.8	0.62
	Shijiazhuang	Jan	627	15.24	18.54	18.74	18.7	0.57
		Jun	692	69.53	71.78	53.15	76.14	0.65
	Tianjin	Jan	629	10.83	17.05	11.78	19.36	0.48
		Jun	675	100.42	143.31	52.22	69.48	0.74

787

788

789

790

791

792

793

794

795

796

797

798

799

800

801

802

803

804

805

806

807

808

809

810

811

812

813

814

815

816

817

818

819

820



821

Table 3. The brute force sensitivity tests set in this study

Abbreviation	Brute force sensitivity test
1 ZI	Zero-out of industry emission sector
2 ZP	Zero-out of power plants emission sector
3 ZT	Zero-out of transport emission sector
4 ZR	Zero-out of residential emission sector
5 A20%-BHTS	20% emission of all anthropogenic sectors in BHTS
6 A20%-HER	20% emission of all anthropogenic sectors in the selected high emission regions of BHTS
7 I20%-HER	20% emission of industry sector in the selected high emission regions of BHTS
8 R20%-HER	20% emission of residential sector in the selected high emission regions of BHTS
9 IR20%-HER	20% emission of industry and residential sector in the selected high emission regions of BHTS
10 ITR20%-HER	20% emission of industry, transport, and residential sector in the selected high emission regions of BHTS

822